ELSEVIER

Earth and Planetary Science Letters 197 (2002) 65–81

EPSL

www.elsevier.com/locate/epsl

Thallium isotope variations in seawater and hydrogenetic, diagenetic, and hydrothermal ferromanganese deposits

Mark Rehkämper [a,*], M. Frank [a], J.R. Hein [b], D. Porcelli [a], A. Halliday [a], J. Ingri [c], V. Liebetrau [d]

[a] *Institute of Isotope Geology and Mineral Resources, ETH Zürich NO C61, CH-8092 Zürich, Switzerland*
[b] *US Geological Survey, 345 Middlefield Road, Menlo Park, CA 94025, USA*
[c] *Division of Applied Geology, Luleå University of Technology, S-95187 Luleå, Sweden*
[d] *GEOMAR, Wischhofstr. 1–3, D-24148 Kiel, Germany*

Received 13 September 2001; received in revised form 10 December 2001; accepted 18 December 2001

Abstract

Results are presented for the first in-depth investigation of Tl isotope variations in marine materials. The Tl isotopic measurements were conducted by multiple collector-inductively coupled plasma mass spectrometry for a comprehensive suite of hydrogenetic ferromanganese crusts, diagenetic Fe–Mn nodules, hydrothermal manganese deposits and seawater samples. The natural variability of Tl isotope compositions in these samples exceeds the analytical reproducibility (±0.05‰) by more than a factor of 40. Hydrogenetic Fe–Mn crusts have ε^{205}Tl of +10 to +14, whereas seawater is characterized by values as low as −8 (ε^{205}Tl represents the deviation of the ^{205}Tl/^{203}Tl ratio of a sample from the NIST SRM 997 Tl isotope standard in parts per 10^4). This ~2‰ difference in isotope composition is thought to result from the isotope fractionation that accompanies the adsorption of Tl onto ferromanganese particles. An equilibrium fractionation factor of $\alpha \sim 1.0021$ is calculated for this process. Ferromanganese nodules and hydrothermal manganese deposits have variable Tl isotope compositions that range between the values obtained for seawater and hydrogenetic Fe–Mn crusts. The variability in ε^{205}Tl in diagenetic nodules appears to be caused by the adsorption of Tl from pore fluids, which act as a closed-system reservoir with a Tl isotope composition that is inferred to be similar to seawater. Nodules with ε^{205}Tl values similar to seawater are found if the scavenging of Tl is nearly quantitative. Hydrothermal manganese deposits display a positive correlation between ε^{205}Tl and Mn/Fe. This trend is thought to be due to the derivation of Tl from distinct hydrothermal sources. Deposits with low Mn/Fe ratios and low ε^{205}Tl are produced by the adsorption of Tl from fluids that are sampled close to hydrothermal sources. Such fluids have low Mn/Fe ratios and relatively high temperatures, such that only minor isotope fractionation occurs during adsorption. Hydrothermal manganese deposits with high Mn/Fe and high ε^{205}Tl are generated by scavenging of Tl from colder, more distal hydrothermal fluids. Under such conditions, adsorption is associated with significant isotope fractionation, and this produces deposits with higher ε^{205}Tl values coupled with high Mn/Fe.

* Corresponding author: Tel.: +41-1-632-7922; Fax: +41-1-632-1179.
E-mail address: markr@erdw.ethz.ch (M. Rehkämper).

0012-821X/02/$ – see front matter
PII: S0012-821X(02)00462-4

Keywords: stable isotopes; isotope fractionation; thallium; ferromanganese composition; sea water

1. Introduction

The search for anomalies in the abundance of ^{205}Tl in meteorites due to the decay of now-extinct ^{205}Pb ($t_{1/2} \sim 15$ Myr) has been the primary motivation of most Tl isotope studies conducted during the past 30 yr [1–6]. A few of these studies also analyzed various terrestrial samples for Tl isotope variations caused by mass-dependent fractionation processes, but they were unable to resolve differences [2,7]. This observation can be readily understood in the context of the following. First, Tl is one of the heaviest naturally occurring elements with two nuclides, ^{203}Tl and ^{205}Tl, that have a mass spread of only about 1%. Differences in isotope composition due to fractionation processes are thus expected to be relatively small. Second, all older Tl isotope studies were conducted by thermal ionization mass spectrometry which is unable to achieve the measurement precision required to resolve small (permil level) variations of Tl isotope compositions.

Similar analytical difficulties have long rendered the search for natural variations in the stable isotope compositions of most elements with atomic masses >40 amu very difficult. With only a few exceptions, past stable isotope studies have thus been restricted to a few light elements (e.g. C, O, S). The advent of multiple collector-inductively coupled plasma mass spectrometry (MC-ICPMS) has ameliorated this limitation. This technique permits stable isotope ratio measurements of 'heavy' elements at a level of precision that is sufficient for the resolution of small isotopic variations [8]. Accordingly, MC-ICPMS investigations of natural fractionations of elements such as Fe, Cu, Zn and Mo have attracted significant interest in the last 3 yr [9–11].

In a reconnaissance study, Rehkämper and Halliday [12] measured the Tl isotope compositions of five terrestrial rock samples and the Allende carbonaceous chondrite using MC-ICPMS. Three igneous rocks and the Allende meteorite were found to display small (<0.4‰) but significant differences in their Tl isotope composition. Two ferromanganese crusts furthermore displayed fractionations of up to about 1‰. Thallium is thus the heaviest element for which natural isotope fractionations have been identified.

Based upon this result, we have performed an in-depth investigation of Tl isotope variations in ferromanganese crusts and nodules, hydrothermal manganese deposits and seawater. For these samples, we determine an overall variation in Tl isotope compositions that exceeds 2‰. The analyses were conducted using improved chemical separation and MC-ICPMS measurement protocols that permit reliable Tl isotope ratio measurements with a reproducibility (2σ) of better than ± 0.05‰. The natural variability of the Tl isotope composition thus exceeds the analytical reproducibility by more than a factor of 40.

2. Samples

A total of 38 samples were analyzed, and brief sample descriptions, including locations and water depths, are given in Table 1. The sample suite comprises ferromanganese (Fe–Mn) crusts and nodules, hydrothermal manganese deposits and three seawater samples. The deposits are categorized by their geochemistry, mineralogy and texture as hydrogenetic, diagenetic (mostly mixed diagenetic/hydrogenetic), hydrothermal, and mixed hydrothermal/hydrogenetic. Sample MW8801 is classified as a mixed hydrothermal/hydrogenetic Fe–Mn crust based on its similarity with sample Vulcan 5 D34-39 with respect to its Tl isotope composition and concentration (Table 1). The Fe–Mn crusts and nodules were selected to obtain a global dataset, whereas the hydrothermal deposits were chosen to cover different tectonic settings (ridge, arc, hotspot).

For the Fe–Mn crusts and some of the nodules, only the most recent growth layers were sampled to a depth of 0.5–2 mm. Most bulk samples were received as powders and analyzed without further

preparation. Otherwise, bulk sample powders were prepared by manual grinding of small sample chunks in an agate mortar. The seawater samples were acidified to a pH of 2 directly after collection using concentrated HCl. The surface seawater sample from Tenerife, which was collected directly off the shoreline, was filtered through a 0.45 μm Millipore filter prior to analysis. The two Arctic Ocean seawater samples were analyzed without prior filtration.

3. Analytical methods

For the ferromanganese deposits, approximately 2–100 mg of sample powder was used for the analyses. The powders were first leached for 15–30 min on a warm hotplate with 6 M HCl and any undissolved (detrital) material was separated from the solution by centrifugation. Following this initial step, the chemical methods applied are similar to those previously described by Rehkämper and Halliday [12]. Only a single pass through a small anion-exchange column (containing 100 μl of AG1 X 8, 200–400 mesh resin), however, was used to obtain purified fractions of Tl and Pb for isotopic analysis. The blanks for Tl and Pb were monitored repeatedly and found to be insignificant at $<0.1\%$ of the extant Tl and Pb in the analyzed sample splits.

A modified version of the ion-exchange chemistry was utilized for the pre-concentration of Tl from the seawater samples. Approximately 1–1.5 l of seawater was acidified with 11 M HCl to obtain a total acid molarity of 0.1 M HCl. Following the addition of 1‰ (v/v) of saturated bromine water, the samples were left to stand for at least 24 h to ensure complete oxidation of Tl^{+} to Tl^{3+}. The seawater was then passed through a column filled with 1 ml of AG1 X 8 (200–400 mesh) anion-exchange resin, which had been cleaned and equilibrated as described by Rehkämper and Halliday [12]. Previous studies have shown that trivalent Tl is quantitatively adsorbed from seawater onto the anion-exchange resin under such conditions [13,14]. The elution of matrix elements and Tl from the resin followed standard procedures [12]. Experiments, which were conducted with seawater samples doped with large quantities of NIST SRM 997 Tl, confirmed that the procedure achieves quantitative adsorption of Tl from seawater and demonstrated that the isotope composition of the isolated Tl is not fractionated with respect to the original sample.

All Tl isotopic measurements were performed with a Nu Plasma MC-ICPMS instrument at the ETH Zürich using techniques adapted from published measurement protocols [12,15]. The methods permit the determination of Tl and Pb isotope compositions as well as Tl concentrations on the same sample aliquot. All Tl isotope data are reported relative to the Tl isotope composition of NIST SRM 997 Tl (National Institute of Standards and Technology Standard Reference Material), which has a $^{205}Tl/^{203}Tl$ isotope ratio of 2.3871 [7]. Owing to the small natural variations, an ε-notation is used as follows:

$$\varepsilon^{205}\mathrm{Tl} = \left(\frac{R_{\mathrm{Sample}}}{R_{\mathrm{Std}}} - 1\right) * 10000 \qquad (1)$$

where R_{Sample} and R_{Std} denote the $^{205}Tl/^{203}Tl$ isotope ratio of the sample and standard, respectively. Positive $\varepsilon^{205}Tl$ values are thus obtained for samples enriched in ^{205}Tl, whereas negative $\varepsilon^{205}Tl$ values denote samples with isotopically light Tl.

Repeated analyses of an Aldrich Tl solution and of an in-house Fe–Mn crust standard were performed to monitor and evaluate the quality of the analytical data. For the Aldrich solution, which was analyzed without chemical processing, an external reproducibility (2σ) of ± 0.29 $\varepsilon^{205}Tl$ units ($n = 14$, where n is the number of analyses on separate measurement sessions) was obtained. For the Fe–Mn crust standard, the external reproducibility is slightly worse at ± 0.45 $\varepsilon^{205}Tl$ units (based on the results of 12 analyses of three separate dissolutions; one dissolution was split into four aliquots that were processed individually through the column chemistry).

The Pb isotope results are reported relative to the Pb isotope composition of Todt et al. [16] for the NIST SRM 981 Pb. The Pb data obtained for the in-house Fe–Mn crust standard indicate an external precision (2σ) of ~ 150 ppm for

Table 1
Data compilation for the samples analyzed in the present study

Cruise or supplier	Sample	Section (mm)	Type	Location	Latitude	Longitude	Water depth (m)	ε^{205}Tl	$^{206}Pb/^{204}Pb$	$^{207}Pb/^{204}Pb$	$^{208}Pb/^{204}Pb$	Tl (ppm)	Mn (%)	Fe (%)
Hydrogenetic deposits														
Alv 539	2-1A	0.5–1	crust	N. Atlantic	35°36.4′N	58°47.1′ W	2665	11.6	19.267	15.682	38.447	53.3	21.0	25.9
Hudson St. 54	BM1969.05	0–2	crust	N. Atlantic	39°0′N	60°57′W	1850	12.5	19.126	15.668	39.222	40.8	19.2	30.4
	Duplicate	0–0.05						12.3	19.299	15.683	39.539	49.0		
Discovery 144	D 10979	0–1	crust	N. Atlantic	32°36.0′N	24°25.0′W	5347–4867	12.6	19.003	15.685	39.098	28.2		
ArcI TR079	D-14	0–1	crust	N. Atlantic	16°55′N	61°10′W	2000	12.3	19.157	15.688	39.280	81.0	22.8	20.5
	BM1963.897	0–1	crust	N. Atlantic	30°58.0′N	78°30.0′W	850	12.8	19.041	15.688	39.029	59.7		
Endeavor EN063	32D	0–1	crust	S. Atlantic	32°11.5′S	32°43.0′W	3310	13.1	18.773	15.656	38.799	29.4		
SO-84	DS43	0–2	crust	S. Atlantic	15°9.0′S	8°21.0′W	1990–1966	14.1	19.092	15.728	39.179	51.5		
TBD 463	6854-6	0–1	nodule	Southern Oc.	37°46.5′S	16°55.1′E	4517	11.3	18.855	15.670	38.884	40.7		
	DR 153	0–1	crust	Southern Oc.	64°57.5′S	91°16.4′W	3300–3150	13.7	18.769	15.636	38.717	91.6		
Antipode	109D-C	0–1	crust	Indian Oc.	27°58.4′S	60°47.7′E	5698–5178	13.9	18.807	15.660	38.869	73.3	19.8	24.2
DODO	232D	0–1	crust	Indian Oc.	5°23.0′S	97°29.0′E	4119	13.6	18.919	15.721	39.215	27.1		
GMAT	14D	0–1	crust	Pacific	13°59′N	96°08′W	4000–3400	12.0	18.703	15.610	38.552	12.2	21.7	22.0
VA13/2	237KD	0–1	crust	Pacific	09°18′N	146°03′W	4830	13.8	18.719	15.633	38.740	80.1	32.8	16.9
F7-87-SC	D9-16	0–1	crust	Pacific	32°15.58′N	121°16.36′W	2300–2235	10.4	18.845	15.646	38.859	38.7		
F10-89-CP	D27-2-1	0–1	crust	Pacific	7°31′N	169°40′E	1670–1570	10.9	18.711	15.630	38.738	42.8		
F7-86-HW	CD29-2	0–1	crust	Pacific	16°42.4′N	168°14.2′W	2390–1970	14.3	18.699	15.641	38.782	19.9	32.1	15.9
F10-89-CP	D11-1	0–2	crust	Pacific	11°39′N	161°41′E	1870–1690	14.1	18.687	15.637	38.756	90.7		
S6-79-NP	D4-13A	0–1	crust	Pacific	53°32.6′N	144°22.4′W	2100	13.7	18.837	15.625	38.691	47.0		
Deep-water diagenetic deposits														
	GeoB1037-2	0–1	nodule	S. Atlantic	13°09.1′S	0°09.0′E	5626	3.3	19.142	15.742	39.256	31.8	30.1	6.7
VA16	13KD-1	0–1	crust	Indian Oc.	12°54.4′S	119°52.6′E	2100	8.6	18.816	15.669	39.002	35.1	28.0	12.0
DOMES A	Mn164: DJ18	0–1	nodule	Pacific	9°25.6′N	151°31.2′W	5160	4.3	18.718	15.633	38.741	103		
DOMES A	Mn192: DJ48	0–1	nodule	Pacific	9°22.0′N	151°25.9′W	5165	2.3	18.718	15.634	38.740	122		
USGS	Nod-A-1	bulk	nodule	Atlantic	31°02′N	78°22′W	788	8.9	18.957	15.675	38.929	108	18.5	10.9
USGS	Nod-P-1	bulk	nodule	Pacific	14°50′N	124°28′W	4300	0.5	18.697	15.629	38.669	146	29.1	5.8
GSJ	JMn-1	bulk	nodule	Pacific	0°47.2′S	166°07.1′W	5212	6.2	18.760	15.633	38.724	177	25.6	10.1
Shallow-water diagenetic deposits														
	82-43-108	bulk	micro-nodules	Gulf of Bothnia	64°05′N	21°25′E	94	−0.2	20.710	15.868	39.390	15.8	30.2	5.6
	Duplicate							−0.2	20.817	15.880	39.463	19.5		
	MB99IS1	bulk	encru-station	SW Baltic Sea	54°10′N	11°21′E	22	−5.2	18.893	15.676	38.647	5.35		
	Duplicate							−5.3	18.893	15.676	38.649	5.40		

Table 1 (*Continued*)

Cruise or supplier	Sample	Section (mm)	Type	Location	Latitude	Longitude	Water depth (m)	ε^{205}Tl	$\frac{^{206}Pb}{^{204}Pb}$	$\frac{^{207}Pb}{^{204}Pb}$	$\frac{^{208}Pb}{^{204}Pb}$	Tl (ppm)	Mn (%)	Fe (%)
Hydrothermal deposits														
L3-84-SP	D1-17-IV	bulk	hydroth. dep.	Lau Basin	22°17.78′S	176°38.89′W	2063–1965	7.0	18.771	15.628	38.677	0.95	50.3	0.44
L3-84-SP	D17-1-IV	bulk	hydroth. dep.	Tonga Ridge	23°24.28′S	175°51.29′W	1710–1200	−2.6	18.764	15.634	38.702	3.45	40.7	2.51
F11-90-CP	D11-9-3	bulk	hydroth. dep.	Yap Arc	8°55.21′N	137°41.01′E	2300–2280	−3.0	18.667	15.629	38.725	44.0	49.1	1.82
F11-91-HW	1-D1-1B	bulk	hydroth. dep.	Hawaii	20°37.4′N	155°49.4′W	1800–1310	−5.9	18.662	15.633	38.732	11.7	52.3	1.49
Pleiades II	D5-1A	bulk	hydroth. dep.	Galapagos R.	0°36′N	86°08.82′W	3822	4.1	18.849	15.652	38.780	0.68	54.5	0.47
TT192	D3-3-II	bulk	hydroth. dep.	Mariana Arc	17°09′N	145°39′E	2975–2860	0.0	18.830	15.639	38.708	8.54	53.6	0.71
Mixed hydrothermal/hydrogenetic deposits														
Vulcan 5	D34-39	0–1	crust	Southern Oc.	57°46.91′S	07°40.29′W	3983–3648	10.3	18.856	15.658	38.928	9.48	8.05	20.7
MW8801	D18-1	0–1	crust	Southern Oc.	50°02.4′S	126°44.51′E	3993	7.7	18.794	15.638	38.858	7.00		
Seawater														
Tenerife 01	TSW		seawater	N. Atlantic	28°30′N	16°17′W	0	−8.1						
Arctic 2000	St. 3, 5 m		seawater	Arctic Oc.	75°11′N	149°56′W	5	−5.2						
Arctic 2000	St. 3, 2000 m		seawater	Arctic Oc.	75°11′N	149°56′W	2000	−5.7						

The Fe and Mn concentrations are from [28] and M. Frank, unpublished results (hydrogenetic Fe–Mn crusts, GeoB1037-2, VA16 13KD-1), [40,41] (USGS and GSJ samples), J. Ingri, unpublished results (Baltic micronodules), J.R. Hein, unpublished results (hydrothermal deposits), and [26] (Vulcan 5 D34-39).

$^{206}Pb/^{204}Pb$, $^{207}Pb/^{204}Pb$, and $^{208}Pb/^{204}Pb$. The Tl concentrations are estimated to have a precision and accuracy of ~10–25% and this is sufficient for the purposes of this study.

4. Results

The Tl isotope results obtained for the Fe–Mn deposits and seawater samples (Table 1) are plotted in diagrams of ε^{205}Tl vs. Tl concentration and ε^{205}Tl vs. Mn/Fe in Fig. 1a,b. It is noteworthy that the different deposit types occupy distinct fields that have only minor overlap in both diagrams.

4.1. Hydrogenetic ferromanganese crusts and seawater

The hydrogenetic Fe–Mn crusts (including the nodule TBD 463 6854-6) are characterized by the heaviest Tl isotope compositions, with ε^{205}Tl values that fall into a narrow range between +10.0 and +14.5 (Table 1, Fig. 1). The Tl concentrations are observed to vary from 10 to 90 ppm, with an average abundance of about 50 ppm (Fig. 1a). Our analyses yield lower Tl concentrations for Fe–Mn crusts than previous studies [17] and it is likely that this mainly is an artifact of our sampling techniques. First, only the most recent surface layers of the Fe–Mn crusts were sampled, and the sample powders were ubiquitously contaminated with the resin that was used to preserve the structure of the bulk crusts. Second, the samples were not dried to remove hygroscopic water prior to weighing. Third, the samples were only leached, rather than totally dissolved for analysis. In the following, we assume that ferromanganese crusts display a range in Tl abundances (30–200 ppm) that is similar to nodules, in accordance with the results of previous studies [17]. In Fig. 1b, the Fe–Mn crusts occupy a distinct field, because they are characterized by both low Mn/Fe ratios (~0.5–2) and high ε^{205}Tl values.

The seawater samples display, on average, the lowest ε^{205}Tl values. The lightest Tl isotope composition was measured for the seawater sample collected in the North Atlantic off Tenerife, which has ε^{205}Tl ~ −8. The two other seawater samples, which were collected at different depths at a single location in the Arctic Ocean, have Tl isotope compositions that are identical within error at ε^{205}Tl ~ −5.5 (Table 1). The minor difference in Tl isotope compositions between the Atlantic and the two Arctic Ocean samples may indicate small variations of Tl isotope ratios in the oceans. Large differences in ε^{205}Tl are not expected, because Tl has an estimated global oceanic residence time of about $1–3\times10^4$ yr [18,19]. The observed variations may nonetheless reflect distinct continental inputs because (1) the Arctic Ocean basin

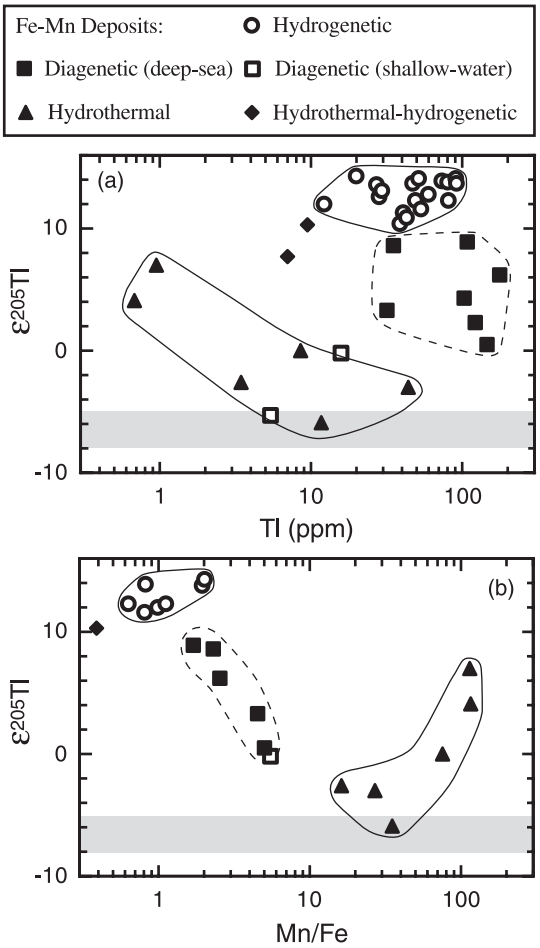

Fig. 1. Plots of (a) ε^{205}Tl vs. Tl concentration and (b) ε^{205}Tl vs. Mn/Fe ratio for the samples analyzed in this study. Note the logarithmic scales. The shaded field denotes the range of Tl isotope compositions for seawater samples (ε^{205}Tl ~ −5 to −8).

is relatively isolated and (2) the Tenerife seawater was collected directly off the coast of the island. It is unlikely that the difference is related to the presence of particulates in the unfiltered Arctic Ocean samples, because sample collection was performed in a permanently ice-covered area where the water has very low particle concentrations.

4.2. Diagenetic ferromanganese deposits

The diagenetic/hydrogenetic deep-sea Fe–Mn nodules and crusts (simply termed deep-water diagenetic deposits in the following) exhibit a much larger range of Tl isotope compositions than the hydrogenetic ferromanganese crusts, with ε^{205}Tl values of between 0 and +9 (Fig. 1, Table 1). Within this group of samples, one of the highest ε^{205}Tl values is displayed by the Fe–Mn crust VA16 13KD-1, which has recent growth layers that show a clear diagenetic signature in both major and minor element contents (M. Frank, unpublished results). The deep-water deposits have Tl concentrations that vary from 30 to almost 200 ppm (Fig. 1a), in accordance with the results of previous nodule studies [17]. The samples also show a good correlation ($r = 0.97$) of increasing ε^{205}Tl with decreasing Mn/Fe ratio (Fig. 1b).

The two shallow-water diagenetic deposits from the Baltic Sea have ε^{205}Tl values of 0 and −5, coupled with relatively low Tl concentrations of only about 17 and 5 ppm, respectively. Thus, they plot in a field that is distinct from the diagenetic deep-water deposits in Fig. 1a, at low ε^{205}Tl and low Tl abundances.

4.3. Hydrothermal manganese deposits

The six hydrothermal manganese deposits are similar to the diagenetic samples, in that ε^{205}Tl ranges between the values obtained for seawater and hydrogenetic Fe–Mn crusts. The range of Tl concentrations is large, with abundances varying from 0.7 to 44 ppm (Fig. 1, Table 1). The hydrothermal deposits define a trend in Fig. 1a, in which the samples with the lowest Tl concentrations have the heaviest Tl isotope compositions. A positive correlation is observed between ε^{205}Tl and Mn/Fe, whereas the deep-sea diagenetic deposits show a negative trend, albeit at much lower Mn/Fe ratios (Fig. 1b).

The mixed hydrothermal/hydrogenetic Fe–Mn crusts are characterized by Tl (and Pb) isotope compositions and Tl concentrations that are intermediate with respect to 'pure' hydrothermal and hydrogenetic ferromanganese deposits (Fig. 1a, Table 1). These samples will not be discussed explicitly in the following, because they are assumed to form either by a process that is intermediate between the hydrothermal and hydrogenetic growth mechanisms or a combination of these two processes.

5. Discussion

5.1. The relationship between seawater and hydrogenetic ferromanganese crusts

One of the key results of this study is the lack of a correlation between the (non-radiogenic) isotope ratio of Tl and the radiogenic isotope com-

Table 2
Tl isotope ratios and concentrations of hydrogenetic Fe–Mn crusts and seawater

	ε^{205}Tl	Tl
Hydrogenetic Fe–Mn Crusts – range	+10.4 – +14.3	12 – 200 ppm
Seawater – range	−5.2 – −8.1	2 – 20 ppt
Hydrogenetic Fe–Mn crusts – preferred	14.0	90 ppm
Seawater – preferred	−7	15 ppt
	Fractionation factor (α)	Tl distribution coefficient (D)
Hydrogenetic Fe–Mn crusts – seawater	1.0021	6×10^6

These values were used to calculate the equilibrium fractionation factor and apparent bulk distribution coefficient of Tl for the adsorption from seawater onto ferromanganese deposits.
The Tl concentrations of seawater are from [18,50,51].

positions of Pb, despite significant variability of the latter (Fig. 2, Table 1). A comparison with the Nd [20–25] and Hf [21,26] isotope data of previous studies on the same samples also shows no correlation with ε^{205}Tl. In addition, there is no clear difference in Tl isotopes for samples collected at different water depths. Furthermore, there is no systematic variation of ε^{205}Tl values for samples collected in different ocean basins or co-variation of ε^{205}Tl with radiogenic isotopes within a single ocean basin (Fig. 2). Thus, ε^{205}Tl does not change systematically with sample location. Taken together, these results provide evidence for a complete decoupling between the processes that govern radiogenic isotope distributions and those that control variations in ε^{205}Tl for Fe–Mn crusts. This interpretation contrasts with the results of a time series (6–0 Ma) Fe isotope study of a North Atlantic Fe–Mn crust that showed a good correlation between changes in Pb and stable Fe isotope compositions [27]. The interpretation that Tl isotope variations are not influenced by the processes that determine variations in radiogenic isotope compositions, such as differences in continental input into the oceans [28], is not surprising. As with the Li isotope system, the Tl isotope variations appear to be governed by local fractionations rather than global distribution processes.

The second striking feature of the dataset for hydrogenetic Fe–Mn crusts is the limited range of Tl isotope compositions, which are uniformly heavier than seawater by about 2‰ (Fig. 1). The data for hydrogenetic crusts appear to define an upper limit in ε^{205}Tl of approximately +14 to +14.5 ε^{205}Tl units. Hydrogenetic Fe–Mn crusts grow at a rate of ~1–10 mm/Myr, probably by precipitation of Mn- and Fe-oxide particles from seawater and scavenging of trace elements from the water column [17]. Therefore, it is likely that the Tl is displaying isotopic equilibrium fractionation. The equilibrium fractionation factor α can be calculated by comparing the Tl isotope data obtained for seawater and Fe–Mn crust samples. Using values compiled in Table 2, the fractionation factor is estimated to be $\alpha = 1.0021$. Similarly, the concentration of Tl in seawater and ferromanganese crusts can be used to estimate a

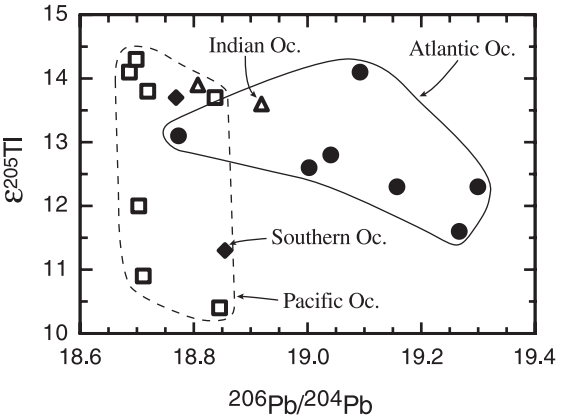

Fig. 2. Plot of ε^{205}Tl versus ^{206}Pb/^{204}Pb for the hydrogenetic ferromanganese crusts only. Different symbols denote samples from different ocean basins.

bulk distribution coefficient D for Tl between these two phases (Table 2). The uncertainty of the D value, however, is significantly larger then the uncertainty of α, due to the larger variability of Tl concentrations in the Fe–Mn crusts.

Two different mechanisms that could be responsible for the differences in Tl isotope composition between seawater and Fe–Mn crusts are possible. First, isotopic fractionation between Tl(I) and Tl(III) may occur in seawater. Second, the Tl isotope fractionation may take place during adsorption on the surface of the Fe–Mn crusts. A number of factors argue for the second interpretation. Thermodynamic calculations show that Tl should occur primarily as Tl(I) in seawater [29]. If the isotope fractionation is generated by dissolved Tl species with different redox states, mass balance considerations thus require the minor species (Tl^{3+}) to be enriched in ^{205}Tl. In this case, preferential adsorption of Tl(III) characterized by high ε^{205}Tl would be responsible for the heavy Tl isotope signatures of Fe–Mn crusts. Leaching studies, however, show that Tl is mainly associated with Mn-oxide phases in ferromanganese crusts. This suggests that Tl is scavenged as a monovalent cation from seawater, because Tl^{3+} would be more readily adsorbed by Fe-oxides [30]. These observations indicate that the isotope fractionation of Tl occurs due to the preferential adsorption of $^{205}Tl^{+}$ from seawater onto Mn-oxide particulates, possibly because this isotope dis-

plays stronger bonding to the particle surface than $^{203}Tl^{+}$. It is notable that similar surface adsorption and ion-exchange processes produce isotopic fractionation for elements such as Li and Fe in both natural and laboratory systems [31,32].

5.2. The relationship between Fe–Mn crusts and deep-sea diagenetic Fe–Mn nodules

The deep-sea diagenetic Fe–Mn crusts and nodules have uniformly lighter Tl isotope compositions than the hydrogenetic samples. The ε^{205}Tl values of the deep-water diagenetic deposits furthermore display a negative correlation with Mn/Fe ratio (Fig. 1b). This indicates that nodules with a particularly strong diagenetic character and high Mn/Fe also have comparatively low ε^{205}Tl values. These observations can be explained by continuous adsorption of Tl onto Mn-oxide surfaces in a closed-system reservoir of limited size (Fig. 3). Pore fluids, which are known to be an important source of metals for diagenetic ferromanganese nodules [33], can represent such a closed-system reservoir if adsorption is fast and the fluids are sufficiently stagnant. In this case, the adsorption of Tl from a batch of liquid onto nodule surfaces can significantly deplete the fluid in Tl. At the limit of (near-)quantitative scavenging, nodules with Tl isotope compositions identical to the pore fluids are produced.

The adsorption process was modeled for both batch and fractional (Rayleigh) adsorption of Tl. Assuming that the adsorption of dissolved Tl onto the Fe–Mn deposits occurs by batch partitioning, the Tl concentration and isotope composition of the deposits can be calculated as:

$$c_s = \frac{D*c_{1,0}}{x_1 + D(1-x_1)} \quad (2)$$

$$R_s = \frac{\alpha*R_{1,0}}{f_1 + \alpha(1-f_1)} \quad (3)$$

where c_s and $c_{l,0}$ denote the Tl concentration of the solid and the initial liquid; R_s and $R_{l,0}$ are the $^{205}Tl/^{203}Tl$ ratio of the solid and the initial liquid; x_l is the mass fraction of the system that is liquid (or in solution), such that $x_l = 1-x_s$ where x_s is the mass fraction of the solid Fe–Mn-oxides that have precipitated from solution; f_l is the mass fraction of dissolved Tl in the liquid phase; D and α are the bulk distribution coefficient and isotopic fractionation factor of Tl between the solid and the fluid phase, respectively. For the case of fractional (Rayleigh) adsorption of Tl onto the solid phase, the average composition of the solid is given by:

$$c_s = c_{1,0}\frac{1-x_1^D}{1-x_1} \quad (4)$$

$$R_s = R_{1,0}\frac{1-f_1^\alpha}{1-f_1} \quad (5)$$

With these equations, the precipitation of Fe–Mn-oxides and the partitioning of Tl into this solid phase are treated analogous to crystal fractionation with either batch or fractional equilibration between the crystals and the remaining liquid. In contrast to crystal fractionation, however, the mass fraction of the system that can precipitate to form Fe–Mn-oxides is restricted by the amount of dissolved Fe and Mn available in the liquid. Therefore, the modeling has been limited to $x_s = 8000$ ppb. The values of α and D have already been estimated above, using the Tl isotope and concentration data for hydrogenetic Fe–Mn crusts and seawater (Table 2). This permits the application of Eqs. 2–5, to investigate what values of $R_{l,0}$ and $c_{l,0}$ are required to account for the range of Tl isotope compositions and abundances observed in diagenetic Fe–Mn deposits.

The results of these calculations are summarized and compared with the analytical data in Fig. 3a–f. The two bold curves shown in each panel denote the most extreme initial fluid isotope compositions and Tl abundances ($R_{l,0}$ and $c_{l,0}$, respectively) that are required to account for the nodule data. The bold full curves were obtained using seawater-like values of $\varepsilon^{205}Tl_{l,0} = -7$ and $c_{l,0} = 10$ ppb, whereas the bold dashed curves applied $\varepsilon^{205}Tl_{l,0} = -12$ and $c_{l,0} = 50$ ppb. The latter composition may be appropriate for pore fluids given the fluid mobility of Tl in other environments [34,35] (no pore fluid data are available for Tl). It is also not unreasonable to assume a

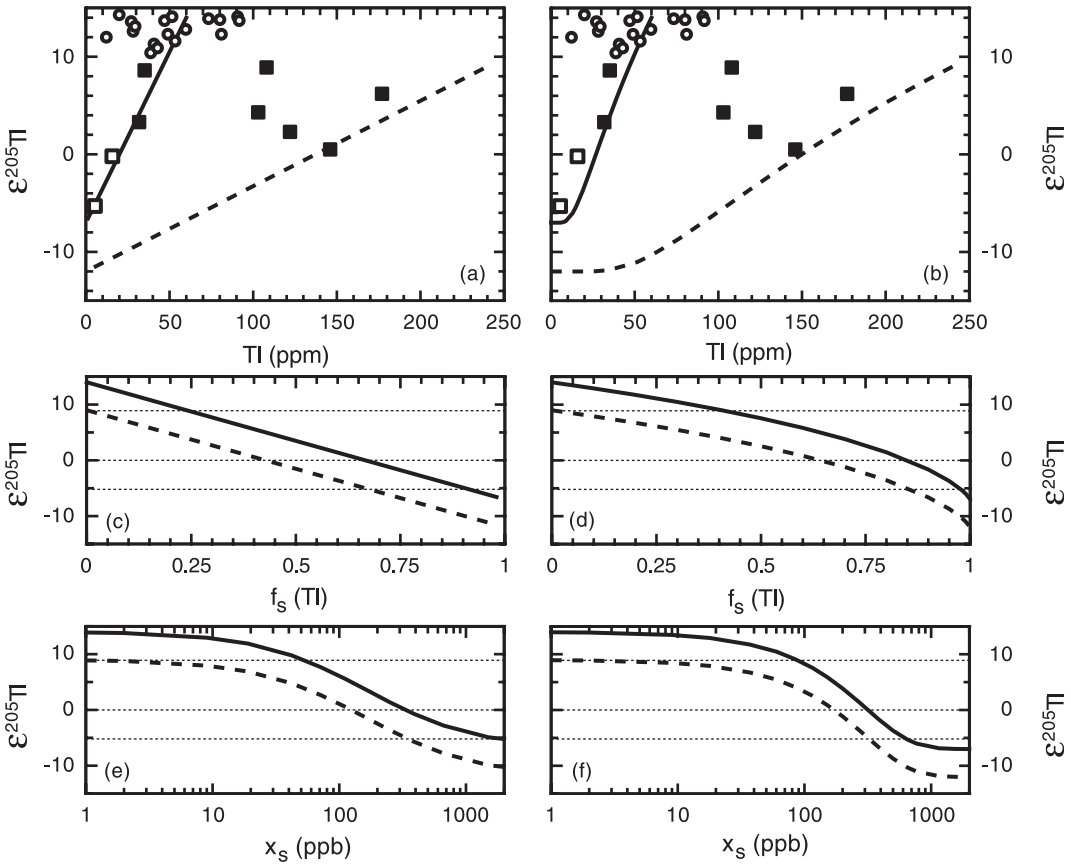

Fig. 3. Results of the modeling that accounts for the Tl isotope compositions of diagenetic Fe–Mn nodules by the adsorption of Tl in a closed-system reservoir. Panels (a), (c), and (e) are for batch adsorption, whereas panels (b), (d), and (f) are for Rayleigh adsorption of Tl. Bold full lines are for an initial fluid with $\varepsilon^{205}\mathrm{Tl} = -7$ and 10 ppb Tl (seawater); bold dashed lines are for an initial fluid with $\varepsilon^{205}\mathrm{Tl} = -12$ and 50 ppb Tl (assumed pore fluid composition). (a,b) Plots of ε^{205}Tl vs. Tl concentration. The data of deep-sea and shallow-water samples are shown as filled and open squares, respectively. Results for hydrogenetic crusts (open circles) are shown for comparison. (c–f) Results of the adsorption models in diagrams of ε^{205}Tl vs. f_s(Tl) and ε^{205}Tl vs. x_s. The parameters f_s(Tl) and x_s denote the mass fraction of Tl (with respect to total Tl) in the solid phase and the mass fraction of the system that has precipitated as a Fe–Mn-oxide phase, respectively. The fine dotted lines show the range of ε^{205}Tl values found in deep-sea (0 to +9) and shallow-water (−5 to 0) diagenetic deposits.

light Tl isotope composition for pore fluids that are in equilibrium with sediments, because isotope fractionation preferentially depletes ^{205}Tl in the liquid phase. The results of the modeling are not critically dependent on the latter assumption, in any case, because very similar results are produced using $c_{l,0} = 50$ ppb combined with $\varepsilon^{205}\mathrm{Tl}_{l,0} = -7$.

The six deep-water diagenetic deposits with intermediate Tl isotope ratios ($\varepsilon^{205}\mathrm{Tl} \sim 0$ to +9) can be explained with the closed-system adsorption model if ~0–80% of the total Tl budget of the initial liquid is partitioned into the solid phase (Fig. 3c,d). Alternatively, the range of ε^{205}Tl values displayed by the deep-sea diagenetic samples can be accounted for by mixing between a diagenetic endmember with low ε^{205}Tl (= 0) and a hydrogenetic endmember with $\varepsilon^{205}\mathrm{Tl} = +14$. Mixing curves between such endmembers are nearly linear or slightly concave upward in Fig. 3a,b. Such mixing processes may be appropriate for deep-sea nodules that are periodically turned and rotated on top of the sediment layer.

The high Tl concentrations of some nodules

(100–200 ppm, Fig. 3a,b) can also be accounted for by applying a higher bulk distribution coefficient for Tl, instead of calling for an initial liquid with a Tl concentration significantly higher than seawater. Application of a D value of between 6×10^6 and 3×10^7 in conjunction with $c_{l,0}=10$ ppb, can also account for all deep-sea diagenetic nodule compositions. Two observations, however, argue against this interpretation. First, this latter model requires very high D values, but Tl concentrations in hydrogenetic crusts are typically <200 ppm [17]. Second, the model cannot readily explain why deep-sea diagenetic deposits with high Mn/Fe ratios typically have low ε^{205}Tl values (Fig. 1b). Variable pore fluid compositions, however, provide a good explanation. The generation of low ε^{205}Tl values requires near-quantitative scavenging of Tl by precipitation of a relatively large mass of solid Fe–Mn-oxides. Up to 300–400 ppb of Fe–Mn-oxides, for example, must precipitate to account for an ε^{205}Tl value of 0 (Fig. 3e,f). Nodules with high Mn/Fe ratios are characteristic of sub-oxic environments and the pore fluids of such settings are typically highly enriched in Mn and Fe [36]. These major elements are thus sufficiently available in solution for precipitation and subsequent adsorption of Tl at high yield.

5.3. Shallow-water diagenetic deposits

To account for the results of the two shallow-water diagenetic deposits with $\varepsilon^{205}\mathrm{Tl}\sim-5$–0, a very large fraction (45–95%) of the dissolved Tl must be adsorbed onto the ferromanganese surfaces from a given batch of fluid (Fig. 3c,d). This requires an ample supply of dissolved Mn and Fe, because up to ~1000 ppb of Fe–Mn-oxides must precipitate to achieve nearly quantitative adsorption of Tl (Fig. 3e,f). Pore fluids from sediments in the Gulf of Bothnia have dissolved Mn and Fe concentrations of up to 2500 μg/l and 7800 μg/l, respectively [37]. This is sufficient to account for the scavenging of Tl at high yield, even if only a partial precipitation of Mn and Fe occurs. Near-quantitative adsorption produces little or no Tl isotope fractionation and low Tl concentrations due to the 'dilution' of Tl in the large volumes of solid that are precipitated (Fig. 3a,b). The latter prediction is in accordance with the analytical results. The Fe–Mn nodules that display the lowest ε^{205}Tl values would therefore also be expected to display the highest growth rates. For the diagenetic ferromanganese deposits analyzed in the present study this indeed appears to be the case. Growth rates of $\sim10^4$ mm/Myr have been determined for the Baltic Sea Fe–Mn encrustation by the Ra–Ba method [38] and values of similar magnitude are likely for the Golf of Bothnia micronodules [37]. In comparison to this, the growth rates of the deep-sea diagenetic samples are orders of magnitude lower. Using the Co-chronometer of Manheim and Lane-Bostwick [39], growth rates of 2–60 mm/Myr are calculated for the five deep-sea diagenetic samples for which Co concentrations were available ([40,41] or unpublished results of M. Frank; Co data were not available for the DOMES samples).

Alternatively, the low ε^{205}Tl values and Tl concentrations of the shallow-water diagenetic samples may also be related to a lower isotope fractionation factor α and/or a lower D value for Tl. Such changes may be reasonable, given the different depositional setting (e.g. higher water temperatures, lower salinity) and conditions (e.g. high growth rates) of the Baltic Sea samples compared to deep-water nodules. Experimental data on the fractionation of Tl isotopes under different conditions of adsorption are required to ultimately resolve this question.

5.4. Tl isotope systematics of hydrothermal manganese deposits

The Tl isotope data of the hydrothermal manganese deposits display positive correlations with 1/Tl (Fig. 4a, $r=0.84$) and Mn/Fe (Fig. 4b, $r=0.91$). This provides important constraints on the processes that are ultimately responsible for the variable ε^{205}Tl values of these samples. The trends of the data in Fig. 4 indicate that Tl is incorporated into the hydrothermal deposits by two endmember processes. Either of these processes can dominate the Tl budget of the samples depending on the local depositional conditions. This can account for the Tl isotope diversity of the hydrothermal deposits if (1) two endmember

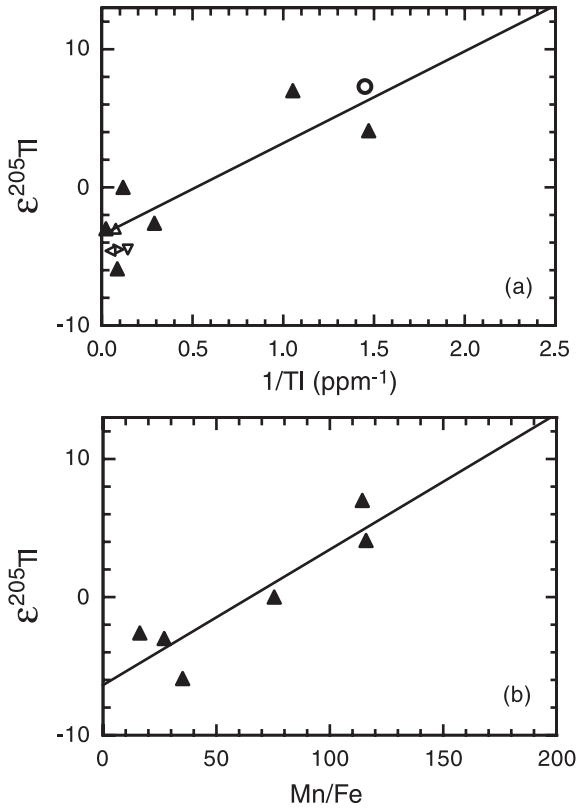

Fig. 4. Plots of (a) ε^{205}Tl vs. 1/Tl concentration and (b) ε^{205}Tl vs. Mn/Fe for the hydrothermal manganese deposits (filled triangles). The straight lines are linear least-squares regressions of the hydrothermal data. In (a) the small open triangles denote the calculated compositions of 'high-Tl' endmembers (models A, C, D, E; Table 3). The open circle denotes the 'low-Tl' endmember of model B (Table 3).

adsorption processes that produce different isotope fractionations are involved and/or (2) each endmember composition derives its Tl from a distinct source reservoir.

The models that are developed in the following produce two endmember hydrothermal deposits that have compositions that lie at or beyond the extremes of the dataset for hydrothermal deposits. The two (hypothetical) endmembers are designated as 'high-Tl' and 'low-Tl' hydrothermal deposits. The 'high-Tl' endmember has a Tl concentration of 5–10 ppm, an ε^{205}Tl value of about -5, combined with an Mn/Fe ratio of 10–40 (Figs. 1 and 4). The 'low-Tl' endmember is assumed to have $\varepsilon^{205}\mathrm{Tl} = +5$. Accordingly, the Tl concentration and Mn/Fe ratio of the 'low-Tl' endmember can be obtained by extending the correlations of the hydrothermal deposits in Fig. 4 to or beyond $\varepsilon^{205}\mathrm{Tl} \sim +5$.

The manganese deposits analyzed in the present study precipitated below the sediment–water interface, from diffuse flows of hydrothermal fluids in the distal part of the hydrothermal system [42]. Both hypothetical endmembers are thus ultimately derived from dilute mixtures of endmember hydrothermal fluids with seawater. This conclusion is further supported by the unradiogenic (mantle-like) Pb isotope ratios (Table 1) and the radiogenic Hf isotope compositions of three samples previously analyzed by Godfrey et al. [26]. The latter study applied rare earth element (REE) patterns to infer that the REE budget of these (and other) hydrothermal deposits was derived from fluids that exhibit a mixing ratio of endmember hydrothermal fluid to seawater of about 1:1000. Such a mixture will have a Mn concentration that is more than three orders of magnitude higher than seawater, but the Tl abundance will only be enhanced by less than a factor of 6 (Table 3). Therefore, the Tl isotope compositions of hydrothermal fluid–seawater mixtures will be similar to seawater unless mixing ratios of $\ll$1:1000 are assumed, and the endmember hydrothermal fluids are extremely Tl-rich and characterized by ε^{205}Tl significantly different from seawater. It is possible that endmember hydrothermal fluids may have ε^{205}Tl values significantly lower than seawater due to preferential leaching of ^{203}Tl from basalts. This is unlikely, however, because high-temperature leaching processes are probably not associated with significant Tl isotope fractionation. The modeling thus assumes a 'normal' endmember hydrothermal fluid with $\varepsilon^{205}\mathrm{Tl} = -9$. A Tl concentration of $\sim$8200 ppb ($\sim$40 nmol/kg) is in accordance with published analytical data [43] but significantly higher Tl abundances of up to 22 500 ppb (110 nmol/kg) have been determined for some endmember hydrothermal fluids [44].

It is conceivable that the observed variations in Tl isotope composition are caused solely by different scavenging or adsorption mechanisms. Studies of natural systems and experiments have shown

that the scavenging of dissolved trace elements by particles operates on a number of distinct timescales. The mechanisms by which a trace element is scavenged can vary as a function of time if scavenging involves different processes (e.g. co-precipitation versus adsorption) or different adsorption sites with distinct reactivities [45,46]. In this scenario, a 'high-Tl' hydrothermal endmember can be derived from a dilute hydrothermal fluid with $\varepsilon^{205}\mathrm{Tl} \sim -5$ by co-precipitation of Tl with the Mn-oxide phase or rapid initial scavenging during Mn precipitation, if these processes are not associated with significant isotope fractionation. The 'low-Tl' endmember could form by 'slow' adsorption of Tl accompanied by isotopic fractionation similar to the process inferred for hydrogenetic Fe–Mn crusts. If this hydrogenetic-type adsorption (with $\alpha = 1.0021$) is assumed to generate a 'low-Tl' endmember with $\varepsilon^{205}\mathrm{Tl} \sim +13$, this deposit should have a Tl concentration of about 0.4 ppm, based on the extrapolation of the data array in Fig. 4a. Mixing of Tl derived by these two endmember processes can account for the variation of ε^{205}Tl and Tl concentration in hydrothermal deposits, because mixing produces linear arrays in Fig. 4a. The hydrothermal deposits with high Tl concentrations have low ε^{205}Tl values because their Tl budget is dominated by the 'high-Tl' endmember, whereas the two hydrothermal deposits with Tl abundances of < 1 ppm can have only a minor contribution of this unfractionated component.

An alternative interpretation of the data for hydrothermal deposits is provided by the assumption that the 'high-Tl' and 'low-Tl' endmembers are each derived from sources with distinct geochemical characteristics. We favor this second interpretation because (1) it does not require undefined processes such as co-precipitation of Tl without isotope fractionation and (2) it provides a reasonable explanation for the positive correlation of ε^{205}Tl with the Mn/Fe ratio (Fig. 1b). In this scenario, the 'high-Tl' endmember is produced by adsorption of Tl from more primitive hydrothermal fluids that have relatively low Mn/Fe and higher temperatures. Such fluids typically emanate relatively close to the hydrothermal source, because dissolved Fe is quickly lost from the liquid phase by oxidation and precipitation [46,47]. Due to the higher temperature of such a hydrothermal fluid compared to ambient bottom water and the temperature dependence of isotope fractionation factors [48], scavenging of Tl should occur with $\alpha < 1.0021$. Adsorption of Tl from a 'normal' dilute hydrothermal fluid assuming $\alpha \sim 1.0005$ can readily produce an appropriate 'high-Tl' endmember (model A, Table 3, Fig. 4a). This model, however, also requires a D value of 6×10^5 and this is an order of magnitude lower than the D value estimated for the adsorption of

Table 3
Results and parameters of the batch adsorption models that are proposed for the origin of endmember hydrothermal deposits

Model	ε^{205}Tl	Tl	Mn	α	D_{eff}	f_s(Tl)	x_s
Endmember hydrothermal fluid	−9	8200 ppt	1.7×10^5 ppb				
1:1000 mix with seawater	−7.7	23 ppt	165 ppb				
A: High-Tl endmember	−3.0	13 ppm		**1.0005**	6×10^5	0.05	∼100 ppb
B: Low-Tl endmember	+7.3	0.69 ppm		**1.0015**	$\mathbf{3 \times 10^4}$	0.001	∼30 ppb
C: High-Tl endmember	−4.6	21 ppm		1.0021	$\mathbf{6 \times 10^6}$	**0.85**	**∼900 ppb**
Endmember hydrothermal fluid	**−30**	8200 ppt	1.7×10^5 ppb				
1:1000 mix with seawater	−15	23 ppt	165 ppb				
D: High-Tl endmember	−4.5	7 ppm		1.0021	6×10^5	**0.50**	**∼1700 ppb**
Endmember hydrothermal fluid	−9	**22 500 ppt**	1.7×10^5 ppb				
1:300 mix with seawater	−8.7	90 ppt	548 ppb				
E: High-Tl endmember	−4.5	11 ppm		1.0021	6×10^5	**0.80**	**∼7000 ppb**
Seawater	−7	15 ppt	0.15 ppb				

All calculations were performed assuming batch adsorption, but fractional (Rayleigh) adsorption produces very similar results. The Tl and Mn concentrations of endmember hydrothermal fluids are in accordance with results presented in [43,44]. D_{eff} is the effective bulk distribution coefficient of Tl. The parameters f_s(Tl) and x_s denote the mass fraction of Tl (with respect to total Tl) in the solid phase and the mass of Fe–Mn-oxides that have precipitated from solution, respectively.

Tl by hydrogenetic crusts (Table 2). The high Mn flux of vent fluids and/or the high growth rates of hydrothermal manganese deposits may be responsible for this discrepancy. Using the Co-chronometer [39], the two deposits with the lowest Tl concentrations yield growth rates of about 3.5×10^4 mm/Myr. The two deposits with the highest Tl concentrations have growth rates of about 1–5×10^2 mm/Myr (Co data are unpublished results of J.R. Hein). These values far exceed the 1–10 mm/Myr growth rates of hydrogenetic Fe–Mn crusts [17] and this may generate lower effective D values (D_{eff}) for Tl in hydrothermal deposits.

Other adsorption models are less successful in accounting for the composition of the 'high-Tl' endmember (models C–E; Table 3, Fig. 4a). In models C–E, the 'high-Tl' endmember is produced by the nearly quantitative (50–80% yield) adsorption of Tl in a closed-system reservoir and assuming a 'normal' isotope fractionation factor of $\alpha=1.0021$. A closed-system scenario may be realistic for a more proximal deposit because Fe–Mn particles can be recycled through vent systems several times before they are deposited [49]. These models, however, need to apply either a high D value (model C) or require an endmember hydrothermal fluid with extremely low ε^{205}Tl (model D) or a high Tl abundance (model E) to generate endmember deposits with $\varepsilon^{205}\mathrm{Tl}\sim-5$. These assumptions are not unreasonable for Tl, but models C–E also require the precipitation of very large mass fractions ($x_s\sim900$–7000 ppb, Table 3) of solid Fe–Mn-oxides. This may be unrealistic given that dilute hydrothermal fluids are unlikely to have dissolved Mn concentrations of >1000 ppb (~20 μmol/kg).

The generation of a 'low-Tl' endmember with $\varepsilon^{205}\mathrm{Tl}=+5$ requires adsorption associated with isotope fractionation, because it is reasonable to assume that all dilute hydrothermal fluids have ε^{205}Tl values similar to or lower than seawater. The formation of a 'low-Tl' endmember that is similar in composition to the two deposits with the lowest Tl concentrations can be achieved by trace scavenging of Tl ($f_s\sim0.1\%$) and by assuming $\alpha=1.0015$ and $D=3\times10^4$ (model B, Table 3, Fig. 4a). Again, these parameters are reasonable, because the high Mn/Fe ratios of the deposits probably reflect more distal hydrothermal fluids. Such fluids are expected to have high Mn/Fe ratios and temperatures that are lower than those inferred for low-Mn/Fe fluids but higher than ambient bottom water. Such conditions should produce deposits with high Mn/Fe and the isotopic fractionation factor during Tl adsorption is expected to be between 1.005 and 1.0021. The extremely high growth rates of the deposits with low Tl concentrations ($\sim3.5\times10^4$ mm/Myr) can furthermore account for the low effective D value of Tl during adsorption (Table 3).

6. Conclusions

The Tl isotope compositions of hydrogenetic ferromanganese crusts, diagenetic Fe–Mn nodules and hydrothermal manganese deposits display clear differences and systematic trends. The hydrogenetic Fe–Mn crusts are characterized by Tl isotope compositions ($\varepsilon^{205}\mathrm{Tl}\sim+10$ to $+14$) that differ from seawater ($\varepsilon^{205}\mathrm{Tl}\sim-7$) by about 2‰. This difference is thought to result from the isotope fractionation that is associated with the adsorption of Tl onto ferromanganese particles. This interpretation will be verified in the future by laboratory adsorption experiments.

Both diagenetic ferromanganese nodules and hydrothermal manganese deposits have ε^{205}Tl values that range between the results obtained for seawater and hydrogenetic Fe–Mn crusts. For the nodules, this variability can be explained by the adsorption of Tl in a closed-system reservoir of limited size. Pore fluids can represent such a reservoir if the adsorption process is fast and the fluids are sufficiently stagnant. The variable ε^{205}Tl values of hydrothermal manganese deposits are thought to be due to the derivation of Tl from vent fluids with different temperatures because the isotopic fractionation should be lower at higher temperatures. The validity of this model can be checked by laboratory experiments that investigate the temperature dependence of the isotope fractionation factor for the adsorption of Tl onto Fe–Mn particles.

These results demonstrate that the Tl isotope compositions of marine ferromanganese deposits

are sensitive indicators of variations in depositional processes. Thallium isotope studies are thus able to provide some insights into (1) the distribution, behavior and cycling of Tl in the marine environment, (2) the processes that are associated with the formation of ferromanganese deposits and (3) the transport and distribution of trace metals in hydrothermal fields. It is conceivable that similar investigations are possible for other low-temperature environments. Further studies are needed to determine if significant Tl isotope fractionations also occur at higher temperatures. If such variations can be verified, this would permit detailed investigations of the sources and sinks of Tl in hydrothermal systems, active arcs and other high-temperature environments.

Acknowledgements

We are grateful to the Scripps Institute of Oceanography, Oregon State University and the Woods Hole Oceanographic Institute for providing some of the samples. M. Froidevaux is thanked for his help in setting up the Tl seawater chemistry. H. Baur, D.-C. Lee, M. Maier, U. Menet, D. Niederer, F. Oberli, B. Rütsche, A. Süsli, C. Stirling and the rest of the IGMR group are gratefully acknowledged for their help in keeping the mass spec running smoothly, support in the clean lab and fruitful discussions. R. Flegal and two anonymous referees provided encouraging and constructive comments. This study was supported by the Schweizerische Nationalfond (SNF).*[BARD]*

References

[1] E. Anders, C.M. Stevens, Search for extinct lead 205 in meteorites, J. Geophys. Res. 65 (1960) 3043–3047.
[2] J.W. Arden, Distribution of lead and thallium in the matrix of the Allende meteorite and the extent of terrestrial lead contamination in chondrites, Earth Planet. Sci. Lett. 62 (1983) 395–406.
[3] J.W. Arden, G. Cressey, Thallium and lead in the Allende C3V carbonaceous chondrite: A study of the matrix phase, Geochim. Cosmochim. Acta 48 (1984) 1899–1912.
[4] J.M. Huey, T.P. Kohman, Search for extinct natural radioactivity of ^{205}Pb via thallium-isotope anomalies in chondrites and lunar soil, Earth Planet. Sci. Lett. 16 (1972) 401–412.
[5] R.G. Ostic, H.M. El-Badry, T.P. Kohmann, Isotopic composition of meteoritic thallium, Earth Planet. Sci. Lett. 7 (1969) 72–76.
[6] G.J. Wasserburg, M. Busso, R. Gallino, C.M. Raiteri, Asymptotic giant branch stars as a source of short-lived radioactive nuclei in the solar nebula, Astrophys. J. 424 (1994) 412–428.
[7] L.P. Dunstan, J.W. Gramlich, I.L. Barnes, W.C. Purdy, Absolute isotopic abundance and the atomic weight of a reference sample of thallium, J. Res. Natl. Bur. Stand. 85 (1980) 1–10.
[8] M. Rehkämper, M. Schönbächler, C.H. Stirling, Multiple collector ICP-MS: Introduction to instrumentation, measurement techniques and analytical capabilities, Geostand. Newsl. 25 (2001) 23–40.
[9] A.D. Anbar, K.A. Knab, J. Barling, Precise determination of mass dependent variations in the isotopic composition of molybdenum using MC-ICPMS, Anal. Chem. 73 (2001) 1425–1431.
[10] N.S. Belshaw, X.K. Zhu, Y. Guo, R.K. O'Nions, High precision measurement of iron isotopes by plasma source mass spectrometry, Int. J. Mass Spectrom. 197 (2000) 191–195.
[11] C.N. Maréchal, P. Télouk, F. Albarède, Precise analysis of copper and zinc isotopic compositions by plasma-source mass spectrometry, Chem. Geol. 156 (1999) 251–273.
[12] M. Rehkämper, A.N. Halliday, The precise measurement of Tl isotopic compositions by MC-ICPMS: Application to the analysis of geological materials and meteorites, Geochim. Cosmochim. Acta 63 (1999) 935–944.
[13] G.E. Batley, T.M. Florence, Determination of thallium in natural waters by anodic stripping voltammetry, Electroanal. Chem. Interfac. Electrochem. 61 (1975) 205–211.
[14] A.D. Matthews, J.P. Riley, The determination of thallium in silicate rocks, marine sediments and sea water, Anal. Chim. Acta 48 (1969) 25–34.
[15] M. Rehkämper, K. Mezger, Investigation of matrix effects for Pb isotope ratio measurements by multiple collector ICP-MS: verification and application of optimized analytical protocols, J. Anal. At. Spectrom. 15 (2000) 1451–1460.
[16] W. Todt, R.A. Cliff, A. Hanser, A.W. Hofmann, Evaluation of a ^{202}Pb–^{205}Pb double spike for high-precision lead isotope analysis, in: A.R. Basu, S.R. Hart (Eds.), Earth Processes: Reading the Isotopic Code, Geophysical Monograph, Am. Geophys. Union, Washington, DC, 1996, pp. 429–437.
[17] J.R. Hein, A. Koschinsky, M. Bau, F.T. Manheim, J.-K. Kang, L. Roberts, Cobalt-rich ferromanganese crusts in the Pacific, in: D.S. Cronan (Ed.), Handbook of Marine Mineral Deposits, CRC Press, Boca Raton, FL, 2000.
[18] A.R. Flegal, C.C. Patterson, Thallium concentrations in seawater, Mar. Chem. 15 (1985) 327–331.

[19] A.R. Flegal, S. Sanudo-Wilhelmy, S.E. Fitzwater, Particulate thallium fluxes in the northeast Pacific, Mar. Chem. 28 (1989) 61–75.
[20] K.W. Burton, H.-F. Ling, R.K. O'Nions, Closure of the Central American Isthmus and its effect on deep-water formation in the North Atlantic, Nature 386 (1997) 382–385.
[21] K. David, M. Frank, R.K. O'Nions, N.S. Belshaw, J.W. Arden, The Hf isotope composition of global seawater and the evolution of Hf isotopes in the deep Pacific Ocean from Fe–Mn crusts, Chem. Geol. 178 (2001) 23–42.
[22] M. Frank, B.C. Reynolds, R.K. O'Nions, Nd and Pb isotopes in Atlantic and Pacific water masses before and after closure of the Panama gateway, Geology 27 (1999) 1147–1150.
[23] H.F. Ling, K.W. Burton, R.K. O'Nions, B.S. Kamber, F. von Blanckenburg, A.J. Gibb, J.R. Hein, Evolution of Nd and Pb isotopes in Central Pacific seawater from ferromanganese crusts, Earth Planet. Sci. Lett. 146 (1997) 1–12.
[24] R.K. O'Nions, M. Frank, F. von Blanckenburg, H.-F. Ling, Secular variations of Nd and Pb isotopes in ferromanganese crusts from the Atlantic, Indian and Pacific Oceans, Earth Planet. Sci. Lett. 155 (1998) 15–28.
[25] B.C. Reynolds, M. Frank, R.K. O'Nions, Nd- and Pb-isotope time series from Atlantic ferromanganese crusts: implications for changes in provenance and paleocirculation over the last 8 Myr, Earth Planet. Sci. Lett. 173 (1999) 381–396.
[26] L.V. Godfrey, D.-C. Lee, W.F. Sangrey, A.N. Halliday, V.J.M. Salters, J.R. Hein, W.M. White, The Hf isotopic composition of ferromanganese nodules and crusts and hydrothermal manganese deposits: Implications for seawater Hf, Earth Planet. Sci. Lett. 151 (1997) 91–105.
[27] X.-K. Zhu, R.K. O'Nions, Y. Guo, B.C. Reynolds, Secular variations of iron isotopes in North Atlantic deep water, Nature 287 (2000) 2000–2002.
[28] M. Frank, R.K. O'Nions, J.R. Hein, V.K. Banaka, 60 Myr records of major elements and Pb–Nd isotopes in hydrogenous ferromanganese crusts: Reconstruction of seawater paleochemistry, Geochim. Cosmochim. Acta 63 (1999) 1689–1708.
[29] T.-S. Lin, J.O. Nriagu, Speciation of thallium in natural waters, in: J.O. Nriagu (Ed.), Thallium in the Environment, Wiley, New York, 1998, pp. 31–43.
[30] A. Koschinsky, J.R. Hein, Acquisition of elements from seawater by ferromanganese crusts: Solid phase association and seawater speciation, Geochim. Cosmochim. Acta, 2001 (submitted).
[31] A.D. Anbar, J.E. Roe, J. Barling, K.H. Nealson, Nonbiological fractionation of iron isotopes, Science 288 (2000) 126–128.
[32] L.-H. Chan, M. Kastner, Lithium isotopic compositions of pore fluids and sediments in the Costa Rica subduction zone: implications for fluid processes and sediment contribution to arc volcanoes, Earth Planet. Sci. Lett. 183 (2000) 275–290.
[33] J. Dymond, M. Lyle, B. Finney, D.Z. Piper, K. Murphy, R. Conrad, N. Pisias, Ferromanganese nodules from MANOP Sites H, S, and R – Control of mineralogical and chemical composition by multiple accretionary processes, Geochim. Cosmochim. Acta 48 (1984) 931–949.
[34] P.D. Noll Jr., H.E. Newsom, W.P. Leeman, J.G. Ryan, The role of hydrothermal fluids in the production of subduction zone magmas: Evidence from siderophile and chalcophile trace elements and boron, Geochim. Cosmochim. Acta 60 (1996) 587–611.
[35] B.W. Vink, The behavior of Tl in the (sub)surface environment in terms of Eh and pH, Chem. Geol. 109 (1993) 119–123.
[36] J.J. Sawlan, J.W. Murray, Trace metal remobilization in the interstitial waters of red clay and hemipelagic marine sediments, Earth Planet. Sci. Lett. 64 (1983) 213–230.
[37] J. Ingri, C. Pontér, Iron and manganese layering in recent sediments in the Gulf of Bothnia, Chem. Geol. 56 (1986) 105–116.
[38] V. Liebetrau, A. Eisenhauer, N. Gussone, G. Wörner, B. Hansen, U/Th/Ra/Ba systematics of Baltic Fe/Mn concretions, EOS (Fall Meeting Supplement) 80 (1999) 538–539.
[39] F.T. Manheim, C.M. Lane-Bostwick, Cobalt in ferromanganese crusts as a monitor of hydrothermal discharge on the Pacific sea floor, Nature 335 (1988) 59–62.
[40] K. Govindaraju, 1994 compilation of the working values and sample description of 383 geostandards, Geostand. Newsl. (Special Issue) 18 (1994) 1–158.
[41] N. Imai, S. Terashima, S. Itoh, A. Ando, 1998 compilation of analytical data for five GSJ geochemical reference samples: the 'instrumental analysis series', Geostand. Newsl. 23 (1999) 223–250.
[42] J.R. Hein, A. Koschinsky, P. Halbach, P. Manheim, M. Bau, J.-K. Kang, N. Lubick, Iron and manganese oxide mineralization in the Pacific, in: K. Nicholson, J.R. Hein, B. Bühn, S. Dasgupta (Eds.), Manganese Mineralization: Geochemistry and Mineralogy of Terrestrial and Marine Deposits, Geological Society, London, 1997, pp. 123–138.
[43] S. Metz, J.H. Trefry, Chemical and mineralogical influences on concentrations of trace metals in hydrothermal fluids, Geochim. Cosmochim. Acta 64 (2000) 2267–2279.
[44] K.L. Von Damm, Controls on the chemistry and temporal variability of seafloor hydrothermal fluids, in: S.E. Humphris, R.A. Zierenberg, L.S. Mullineaux, R.E. Thomson (Eds.), Seafloor Hydrothermal Systems, AGU, Washington, DC, 1995, pp. 222–247.
[45] H.W. Jannasch, B.D. Honeyman, L.S. Balistrieri, J.W. Murray, Kinetics of trace element uptake by marine particles, Geochim. Cosmochim. Acta 52 (1988) 567–577.
[46] M.D. Rudnicki, H. Elderfield, A chemical model of the buoyant and neutrally buoyant plume above the TAG vent field, 26 degrees N, Mid-Atlantic Ridge, Geochim. Cosmochim. Acta 57 (1993) 2939–2957.
[47] K.L. Von Damm, J.M. Edmond, B. Grant, C.I. Measures, Chemistry of submarine hydrothermal solutions at 21°N, East Pacific Rise, Geochim. Cosmochim. Acta 49 (1985) 2197–2220.

[48] J.R. O'Neil, Theoretical and experimental aspects of isotopic fractionations, in: J.W. Valley, H.P. Taylor Jr., J.R. O'Neil (Eds.), Stable Isotopes in High Temperature Geological Processes, Reviews in Mineralogy 16, Mineralogical Society of America, Washington, DC, 1986, pp. 1–40.
[49] C.R. German, R.S.J. Sparks, Particle recycling in the TAG hydrothermal plume, Earth Planet. Sci. Lett. 116 (1993) 129–134.
[50] O. Schedlbauer, K.G. Heumann, Biomethylation of thallium by bacteria and first determination of biogenic dimethylthallium in the ocean, Appl. Organometal. Chem. 14 (2000) 330–340.
[51] M.-T. Wei, S.-J. Jiang, Determination of Tl in sea-water by flow injection hydride generation isotope dilution inductively coupled plasma mass spectrometry, J. Anal. At. Spectrom. 14 (1999) 1177–1181.